

Few to Big: Prototype Expansion Network via Diffusion Learner for Point Cloud Few-shot Semantic Segmentation

Qianguang Zhao¹, Dongli Wang², Yan Zhou^{*2}, Jianxun Li³, Richard Irampaye¹

¹ School of Mathematics and Computational Science, Xiangtan University

² School of Automation and Electronics Information, Xiangtan University

³ School of Automation, Shanghai Jiao Tong University

qg_zhao@smail.xtu.edu.cn, wangdl@xtu.edu.cn, yanzhou@xtu.edu.cn, lijx@sjtu.edu.cn, richarcive@gmail.com

Abstract

Few-shot 3D point cloud semantic segmentation aims to segment novel categories using a minimal number of annotated support samples. While existing prototype-based methods have shown promise, they are constrained by two critical challenges: (i) Intra-class Diversity, where a prototype's limited representational capacity fails to cover a class's full variations, (ii) Inter-set Inconsistency, where prototypes derived from the support set are misaligned with the query feature space. Motivated by the powerful generative capability of diffusion model, we re-purpose its pre-trained conditional encoder to provide a novel source of generalizable features for expanding the prototype's representational range. Under this setup, we introduce the **Prototype Expansion Network (PENet)**, a framework that constructs big-capacity prototypes from two complementary feature sources. PENet employs a dual-stream learner architecture: it retains a conventional fully-supervised **Intrinsic Learner (IL)** to distill representative features, while introducing a novel **Diffusion Learner (DL)** to provide rich generalizable features. The resulting dual prototypes are then processed by a **Prototype Assimilation Module (PAM)**, which adopts a novel push-pull cross-guidance attention block to iteratively align the prototypes with the query space. Furthermore, a **Prototype Calibration Mechanism (PCM)** regularizes the final big-capacity prototype to prevent semantic drift. Extensive experiments on the S3DIS and ScanNet datasets demonstrate that PENet significantly outperforms state-of-the-art methods across various few-shot settings. The code is provided in the Appendix.

Introduction

3D point cloud semantic segmentation has wide-ranging applications across various fields, such as autonomous driving (Wang et al. 2025; Fei et al. 2024), robotics (Soori, Arezoo, and Dastres 2023; Hu et al. 2024), and augmented reality (Serenio et al. 2020). While fully supervised learning has achieved numerous improvements in complex scene understanding (Zhang et al. 2024; Lai et al. 2022), its effectiveness is constrained by the need for large-scale, expensive, and fully-annotated datasets. To address this challenge, few-shot 3D point cloud semantic segmentation (**FS-PCS**) has recently attracted increasing attention, enabling models

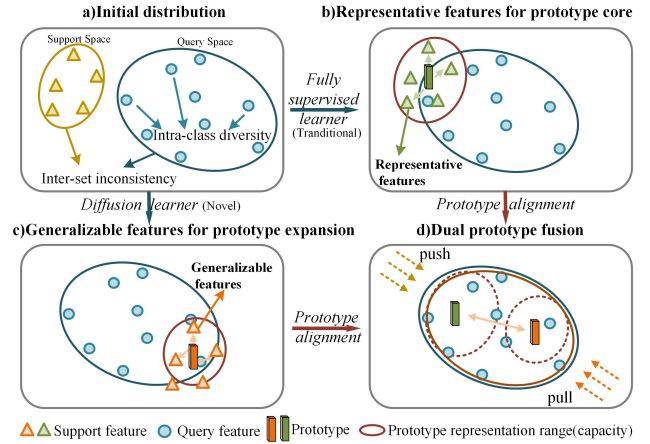


Figure 1: The motivation of proposed approach. a) The initial distribution in FS-PCS presents two challenges: inter-set inconsistency between support and query spaces, and intra-class diversity within the query features. b) A conventional learner yields a prototype with a limited representational range, failing to cover the full class diversity. c) By introducing an additional novel source of generalizable features, the prototype's representational range is significantly expanded. d) The dual prototypes derived from representative and generalizable components are fused and aligned with the query space, resulting in a final big-capacity prototype covers the novel class distribution.

to generalize to unseen novel categories with just a few annotated samples (An et al. 2024; Zhu et al. 2024; He et al. 2023).

Existing FS-PCS methods typically adhere to the meta-learning framework (Vinyals et al. 2016; Snell, Swersky, and Zemel 2017), where prototypes derived from a handful of annotated support samples serve as benchmarks for segmenting unseen query point clouds. However, these prototypical methods face significant challenges due to the inherent sparsity, disorder, and non-structural nature of point clouds (Zhao et al. 2024), which complicates the generation of robust and generalizable prototypes. This difficulty manifests in two critical, intertwined problems: Intra-class Diversity and Inter-set Inconsistency.

Intra-class Diversity, arises because object shapes and ap-

*Corresponding Authors.

pearances can vary dramatically even within the same category (An et al. 2024). Consequently, prototypes distilled from only a few support samples are inherently limited in the richness and diversity of their feature components. We term this limitation the prototype’s representational capacity. In a few-shot setting, prototypes are naturally “small-capacity,” which leads to an insufficient effective representational range, making it difficult to cover the entire distribution of a novel class. While some works attempt to mitigate this by employing multi-prototype strategies (Zhao, Chua, and Lee 2021; Mao et al. 2022), they merely increase the quantity of prototypes without fundamentally expanding their representational capacity.

Simultaneously, these prototypes suffer from Inter-set Inconsistency, a natural distribution gap between the support and query sets that originates from different 3D scenes (Zhu et al. 2023). This gap introduces significant bias when applying support-based prototypes to the query space. Traditional methods rectify this by “pushing” prototypes towards the query distribution through various alignment strategies (Ning et al. 2023; Mao et al. 2022). However, given the significant distribution shift in 3D point clouds, the corrective force of such alignment strategies is often insufficient to fully align the prototype with the query space.

So aforementioned analysis presents a fundamental dilemma: a well-aligned prototype is ineffective if its capacity is too small to cover class diversity, while a big-capacity prototype will fail if it is not properly aligned within the query space. Motivated by these important observations, a pertinent question arises: *How can we leverage a few-shot of support samples to construct aligned big-capacity prototypes for segmenting novel query classes?*

In this paper, we explore expanding the effective representational range of prototypes in few-shot 3D learning scenarios. Our main idea is to enrich the prototype’s feature components to increase its capacity, which we achieve by constructing it from two complementary feature sources. On one hand, we retain the conventional fully-supervised pre-training pipeline to distill representative features. These features provide a stable semantic core for the prototype, ensuring its discriminative power (Figure 1, a→b). On the other hand, we introduce a self-supervised pathway to provide the crucial generalizable features needed for prototype expansion. Motivated by the powerful generative capabilities of diffusion models (Ho, Jain, and Abbeel 2020). These models can recover a complete object shape from pure noise when guided by a condition vector. In this process, the conditional encoder learns to extract robust, holistic geometric priors even from incomplete point cloud inputs. We re-purpose the pre-trained encoder to provide the generalizable features at no extra annotation cost (Figure 1, a→c). Furthermore, to resolve inter-set inconsistency, aforementioned two feature representations must be mutually aligned against the query space distribution before final joint into a single, unified big-capacity prototype (Figure 1, d).

Under this Prototype Expansion setup, we introduce a novel framework, the Prototype Expansion Network (PENet), to effectively address the challenges in FS-PCS by harnessing two complementary feature sources. The overall architecture of PENet is depicted in Figure 2. Given the support and query point clouds, PENet first employs a dual-stream learner architecture to extract two sets of

features: representative features from the **Intrinsic Learner (IL)** and generalizable features from the **Diffusion Learner (DL)** (cost-free). Based on initial prototypes generated from these features, a subsequent **Prototype Assimilation Module (PAM)** is designed to adopt a novel push-pull cross-guidance attention mechanism to iteratively aligns the two sets of prototypes with the query space, providing a more robust corrective force than single-step alignment methods. Subsequently, a Prototype Fusion step combines the aligned dual prototypes into a single big-capacity prototype. Additionally, to ensure the expanded prototype does not deviate from its source semantics, we introduce a **Prototype Calibration Mechanism (PCM)** constrain the final prototype’s ability by reconstructing source support set mask.

- We propose the PENet to address intra-class diversity and inter-set inconsistency in FS-PCS. To the best of our knowledge, this is the first work to explore diffusion model in FS-PCS.
- We design a novel dual-stream architecture features an iterative PAM for robust alignment and a PCM to ensure semantic fidelity.
- Extensive experiments on the S3DIS and ScanNet benchmarks achieving state-of-the-art across various few-shot settings. Our work validates the value of using generative model components for discriminative few-shot learning.

Related Work

Few-Shot 3D Point Cloud Semantic Segmentation.

FS-PCS aims to segment novel classes using a minimal number of annotated support samples. The field was pioneered by AttMPTI (Zhao, Chua, and Lee 2021), which introduced a multi-prototype transductive inference framework. Subsequent research has largely focused on mitigating the discrepancy between support and query distributions (Li et al. 2025). Many works propose to adapt or align support prototypes by incorporating guidance from the query space (Zhang et al. 2023). Other approaches have focused on enhancing feature representations, for instance, by designing modules for bidirectional feature globalization (Huang et al. 2023; Zhang et al. 2023). However, these methods typically rely on a single source of discriminative features. Our work departs from this by introducing a complementary feature stream to fundamentally expand the prototype’s representational capacity.

Diffusion Models for Representation Learning.

Diffusion models have recently achieved state-of-the-art results in generative tasks, including 3D point cloud generation (Lyu et al. 2022; Nichol et al. 2022). Beyond pure generation, their potential for representation learning and discriminative tasks has become an active area of research (Peebles and Xie 2023). One line of work utilizes conditional diffusion models to synthesize labeled data for augmenting training sets in data-scarce scenarios (Gandikota et al. 2023). Another approach employs diffusion models directly as zero-shot classifiers, leveraging their learned data likelihood to predict class probabilities (Li et al. 2023). Furthermore, some studies have demonstrated that the intermediate features of the U-Net denoiser are highly discriminative and can be used for downstream tasks (Bar, Maimon, and Gafni

2022; Huang et al. 2024). In contrast to these methods, our work is the first to re-purpose the pre-trained conditional encoder of a 3D diffusion model as a dedicated feature learner within a few-shot segmentation framework.

Preliminary

Fundamental: Conditional Diffusion Models

Diffusion models (Ho, Jain, and Abbeel 2020; Nichol and Dhariwal 2021) are powerful generative models that operate in two stages: a forward noising process and a reverse generation process. The forward stage is a Markovian process that incrementally adds Gaussian noise to clean data x_0 over T timesteps, defined by $q(x_t | x_{t-1}) = \mathcal{N}(x_t; \sqrt{1 - \beta_t}x_{t-1}, \beta_t \mathbf{I})$. This allows the noised sample x_t to be generated directly from x_0 in a closed form: $q(x_t | x_0) = \mathcal{N}(x_t; \sqrt{\bar{\alpha}_t}x_0, (1 - \bar{\alpha}_t)\mathbf{I})$, where $\alpha_t = 1 - \beta_t$ and $\bar{\alpha}_t = \prod_{i=1}^t \alpha_i$, $\beta_t \in (0, 1)$ is a variance hyperparameter.

The reverse stage learns a neural network p_θ to reverse this process, approximating the true posterior $q(x_{t-1} | x_t)$ by modeling it as a diagonal Gaussian, $p_\theta(x_{t-1} | x_t) = \mathcal{N}(x_{t-1}; \mu_\theta(x_t, t), \sigma_t^2 \mathbf{I})$. In a conditional diffusion model (Zhang, Rao, and Agrawala 2023), this reverse process is guided by a condition vector c , effectively modeling $p_\theta(x_{t-1} | x_t, c)$.

In this work, we do not use the diffusion model for its generative capabilities directly. Instead, we leverage its pre-trained conditional encoder, the component responsible for producing the condition vector c . The encoder enables the extraction of rich, generalizable features even from the few samples in FS-PCS task.

Problem Setup

We follow the standard episodic paradigm for FS-PCS, as established in prior works (Zhao, Chua, and Lee 2021). Each task instance is framed as an N -way K -shot episode, which contains a support set \mathcal{S} and a query set \mathcal{Q} . The support set $\mathcal{S} = \{(X_s^{n,k}, Y_s^{n,k})\}_{n=1, k=1}^{N, K}$ provides N novel classes, where each class n is represented by K annotated samples (shots). The query set $\mathcal{Q} = \{(X_q, Y_q)\}$ consists of an unannotated point cloud that contains instances of the N novel classes. The objective is to leverage the knowledge from the support set \mathcal{S} to predict a point-wise semantic mask for the query point cloud X_q , segmenting it into one of the N target classes or a background category. During meta-training and meta-testing, the set of classes are disjoint ($\mathcal{C}_{\text{train}} \cap \mathcal{C}_{\text{test}} = \emptyset$), forcing the model to learn a generalizable segmentation capability rather than memorizing specific classes.

Methodology

In this section, we first detail our dual-stream Intrinsic and Diffusion Learners; then, we introduce the generation of dual prototypes; next, we present the Prototype Assimilation Module. Finally, we explain how these prototypes are fused and calibrated to construct our PENet framework, as shown in Figure 2.

Prototype Generation

Feature Extractors. Diverging from prior few-shot methods that rely on a single shared feature extraction backbone

(Zhu et al. 2023; Zheng et al. 2024a), our approach processes point cloud inputs through a dual-stream architecture with two distinct learners: the Intrinsic Learner (IL) and the Diffusion Learner (DL), as depicted in Figure 2. The IL extracts representative features by leveraging a fully-supervised pre-training paradigm, while the DL provides complementary generalizable features derived from a self-supervised diffusion process. The synergy between these two feature types provides the rich and diverse components necessary for our prototype expansion. Given the support/query point cloud $X_{s/q} \in \mathbb{R}^{N \times D}$, we use the IL (Φ_{IL}) and DL (Φ_{DL}) to obtain their respective features, given by:

$$\begin{aligned} F_{qi} &= \Phi_{IL}(X_q) \in \mathbb{R}^{N_i \times D_i}, & F_{qd} &= \Phi_{DL}(X_q) \in \mathbb{R}^{N_d \times D_d} \\ F_{si} &= \Phi_{IL}(X_s) \in \mathbb{R}^{N_i \times D_i}, & F_{sd} &= \Phi_{DL}(X_s) \in \mathbb{R}^{N_d \times D_d} \end{aligned} \quad (1)$$

where the resulting $F_{q/si}$ and $F_{q/sd}$ represent the representative and generalizable features, respectively. Note that the learners may operate at different resolutions, resulting in feature maps with different numbers of points (N_i, N_d) and channel dimensions (D_i, D_d).

Intrinsic Learner. Consistent with conventional FS-PCS frameworks, our method retains a fully-supervised feature learner as the Intrinsic Learner (Zhao, Chua, and Lee 2021). This learner is pre-trained via a standard supervised paradigm, enforcing a precise point-to-label mapping (Yu et al. 2021). This process endows the learner with strong discriminative capabilities, allowing it to extract representative features that form a stable semantic core for the prototype. Following the approach in (Zhao, Chua, and Lee 2021), we adopt the widely used DGCNN (Wang et al. 2019) as the backbone for our IL to obtain these features.

Diffusion Learner. While the representative features from the IL provide a strong discriminative foundation, they struggle to generalize across significant intra-class variations. To address this limitation, we introduce a parallel Diffusion Learner in the upper part of Figure 2. The core principle is that an encoder capable of guiding a generative process from pure Gaussian noise to a complete object learned the object’s generalizable geometric priors for prototype expansion. To this end, we re-purpose the pre-trained conditional encoder as our DL. Unlike the IL, which processes the full point cloud, the DL operates on a sparsely masked input. Inspired by PointDif (Zheng et al. 2024b), given an input point cloud $X_{s/q}$, we first partition it into patches and apply a high-ratio random masking. The DL encoder, a multi-layer Transformer, then processes only the visible patches x_i^v . To preserve crucial 3D spatial information, a position embedding function $\psi(\cdot)$, realized by an MLP, generates a positional encoding Pos_i^v for the center coordinate C_i^v of each visible patch. This encoding is fused with the patch features F_i^v and fed into the transformer encoder to extract the latent generalizable features F_d :

$$F_d = \Phi_{DL}(\text{Concat}(F^v, \psi(C^v))) \quad (2)$$

Then generalizable features F_d with masked patch information are aggregated to provide the condition c that guides a denoising diffusion model ϵ_θ to progressively recover the original point cloud from a noisy version z_t . The training

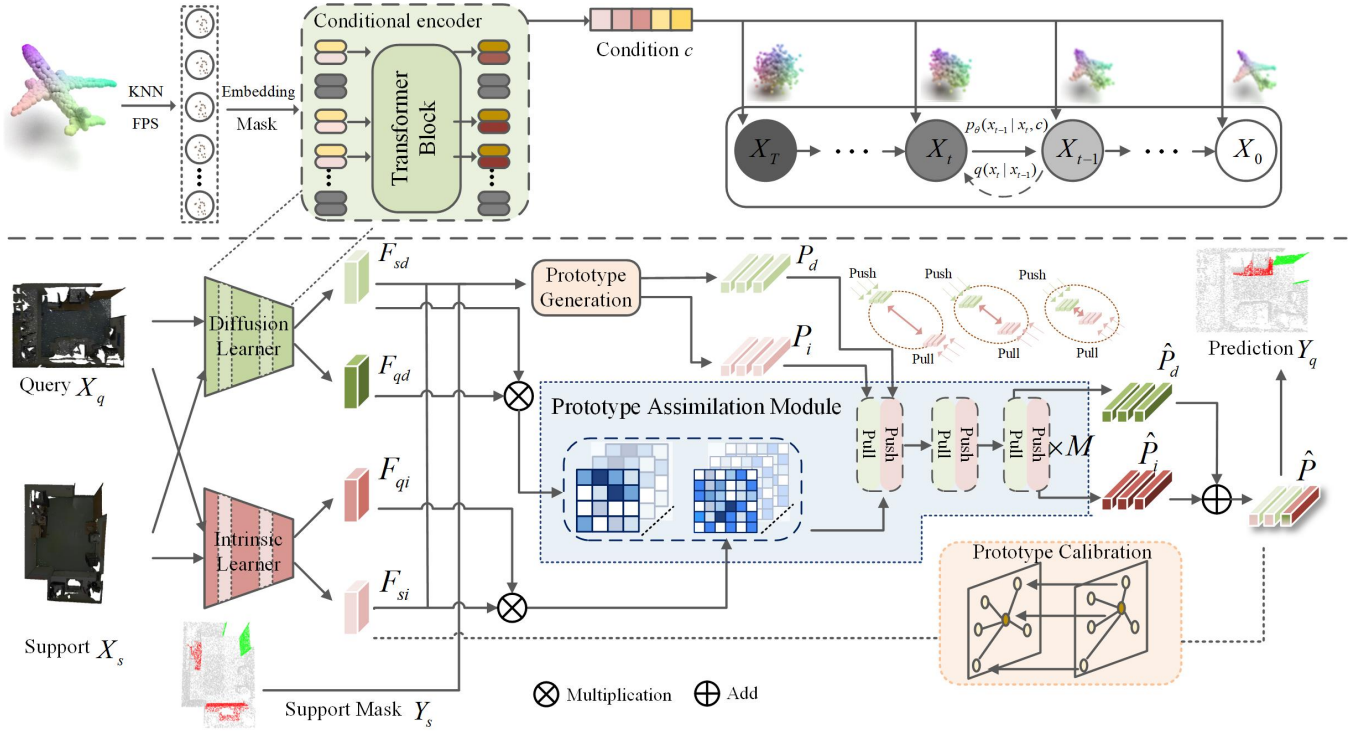


Figure 2: Overall architecture of our proposed PENet. The upper part illustrates the pre-training of the Diffusion Learner’s encoder. In the main framework, given support (X_s) and query (X_q) point clouds, a dual-stream architecture with an Intrinsic Learner (IL) and a Diffusion Learner (DL) extracts representative and generalizable features, respectively. The support features are then used to generate initial dual prototypes (P_i, P_d). These prototypes are forwarded to the Prototype Assimilation Module (PAM), where an iterative push-pull mechanism aligns them with the query space. Subsequently, the aligned prototypes are fused into the final big-capacity prototype (\hat{P}), which is regularized by the Prototype Calibration Mechanism (PCM) to prevent semantic drift.

objective is to minimize the following loss function:

$$\mathcal{L}_{diff} = \mathbb{E}_{x_0, c, \epsilon \sim \mathcal{N}(0, I), t} [\|\epsilon - \epsilon_\theta(z_t, t, c)\|^2] \quad (3)$$

where z_t is the noisy point cloud at timestep t , and ϵ is standard Gaussian noise. To converge under this objective, the DL encoder is compelled to infer the complete object manifold from a highly incomplete input. This local-to-global inference task forces the encoder to learn the underlying structural patterns of a class, rather than surface-level details. These generalizable features provide the rich components necessary for prototype expansion, complementing the representative features from the IL.

Prototype Generation. Contrary to traditional few-shot models that generate prototypes from a single feature source (Zheng et al. 2024a), our method initializes two distinct sets of prototypes by integrating the complementary information from both the representative and generalizable feature streams. This dual-source approach ensures our initial prototypes are endowed with both discriminative power and robust generalizability. Initially, foreground and background prototypes are generated from the annotated support points for both the intrinsic features F_{si} and generalizable features F_{sd} , using farthest point sampling and inverted sample clustering (An et al. 2024). This prototype generation, denoted

as $\text{ProtoGen}(\cdot)$, results in:

$$\begin{aligned} p_c^i, p_{bg}^i &= \text{ProtoGen}(F_{si}, Y_s, L_s), & p_c^i, p_{bg}^i &\in \mathbb{R}^{1 \times D_i} \\ p_c^d, p_{bg}^d &= \text{ProtoGen}(F_{sd}, Y_s, L_s), & p_c^d, p_{bg}^d &\in \mathbb{R}^{1 \times D_d} \end{aligned} \quad (4)$$

where Y_s and L_s are the labels and 3D coordinates of the support set points, respectively. The p_c, p_{bg} are the prototypes for a foreground class c and the background, respectively. Then the C foreground prototypes and the single background prototype are concatenated to form the complete prototype sets:

$$\begin{aligned} P_i &= \text{Concat}(p_1^i, \dots, p_C^i, p_{bg}^i) \in \mathbb{R}^{(C+1) \times D_i} \\ P_d &= \text{Concat}(p_1^d, \dots, p_C^d, p_{bg}^d) \in \mathbb{R}^{(C+1) \times D_d} \end{aligned} \quad (5)$$

where $C + 1$ is the total number of classes in the given N -way setting, including the background.

Prototype Assimilation Module

Having generated the dual prototypes, a critical challenge remains: the inter-set inconsistency between these support-derived prototypes and the query feature distribution, as discussed in Sec. I. To this end, we propose the Prototype Assimilation Module (PAM). As illustrated in Figure 3, PAM

consists of push-pull blocks stacked to operate for N iterations. This mechanism functions figuratively as two interacting corrective forces applied iteratively: a pull force draws the intrinsic prototypes P_i towards the query space of diffusion features, while a symmetric push force drives the diffusion prototypes P_d towards the intrinsic feature space. Through an M -step process, the two prototype sets are jointly assimilated to better align with the query distribution. The core of this module is a cross-guidance channel-wise attention mechanism that directly updates the prototypes.

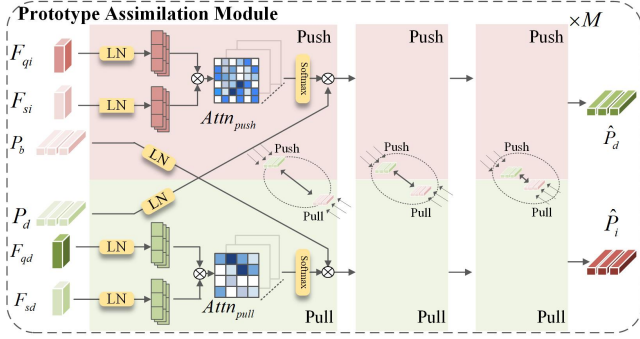


Figure 3: Illustration of Prototype Assimilation Module (PAM).

Pull Operation: Aligning Intrinsic Prototypes via Diffusion Space. The pull operation aims to refine the intrinsic prototypes P_i by leveraging the relational context of the diffusion space. First, we compute a channel-wise attention map $Attn_{pull}$ where the Query and Key are derived from the diffusion-query features F_{qd} and diffusion-support features F_{sd} , respectively:

$$Query_{pull} = (F_{qd})^T W_q, \quad Key_{pull} = (F_{sd})^T W_k. \quad (6)$$

$$Attn_{pull} = \text{softmax} \left(\frac{Query_{pull} \cdot Key_{pull}^T}{\sqrt{D}} \right). \quad (7)$$

where W_q, W_k are learnable linear projection parameters. This attention map, capturing channel-wise dependencies within the diffusion space, then guides the update of the complementary intrinsic prototypes P_i , which serve as the Value:

$$Value_{pull} = P_i W_v. \quad (8)$$

$$P_i^{update} = (Attn_{pull} \cdot Value_{pull}^T)^T. \quad (9)$$

This operation adjusts the intrinsic prototypes along their channel dimensions, infusing them with guidance from the diffusion space. The final aligned intrinsic prototype \hat{P}_i is then obtained via a residual connection and a small MLP $\mathcal{F}_{pull_mlp}(\cdot)$:

$$\hat{P}_i = P_i + \mathcal{F}_{pull_mlp}(P_i^{update}). \quad (10)$$

Push Operation: Aligning Diffusion Prototypes via Intrinsic Space. Symmetrically, the push operation refines the diffusion prototypes P_d using the relational context of the intrinsic space. An intrinsic channel-wise attention map

$Attn_{push}$ is first generated from the intrinsic-query features F_{qi} and intrinsic-support features F_{si} :

$$Query_{push} = (F_{qi})^T W'_q, \quad Key_{push} = (F_{si})^T W'_k. \quad (11)$$

$$Attn_{push} = \text{softmax} \left(\frac{Query_{push} \cdot Key_{push}^T}{\sqrt{D}} \right). \quad (12)$$

This map, encoding representative relationships, is then applied to the complementary diffusion prototypes P_d as the Value:

$$Value_{push} = P_d W'_v. \quad (13)$$

$$P_d^{update} = (Attn_{push} \cdot Value_{push}^T)^T. \quad (14)$$

Finally, a similar residual connection and MLP $\mathcal{F}_{push_mlp}(\cdot)$ are used to obtain the aligned diffusion prototype \hat{P}_d :

$$\hat{P}_d = P_d + \mathcal{F}_{push_mlp}(P_d^{update}). \quad (15)$$

This cross-guidance attention mechanism enables a joint optimization of the dual prototypes. Considering that the generalizable features from the diffusion encoder may operate at a different resolution, the attention map computed within the intrinsic space and the one computed within the diffusion space form a multi-scale correspondence. This allows the prototypes to absorb information from different granularities, leading to a richer final representation.

The final step is to merge these two complementary representations to construct the ultimate big-capacity prototype \hat{P} :

$$\hat{P} = \hat{P}_i + \hat{P}_d \quad (16)$$

The big-capacity prototype is better equipped to cover the full spectrum of intra-class variations, enabling it to more effectively match and identify morphologically diverse samples within the query set.

Prototype Calibration Mechanism

While the prototype assimilation and fusion processes expand the prototype's representational range, they introduce a potential risk: semantic drift. As the prototypes continuously absorb generalizable features and align with the query space, the resulting prototype \hat{P} may deviate from the original class semantics defined by the support samples. To mitigate this issue, we introduce a Prototype Calibration Mechanism (PCM) which ensures the expanded prototype accurately traces back to its origin semantics. Inspired by (He et al. 2023), our calibration mechanism constrains the final prototype \hat{P} to accurately reconstruct the support set mask.

The operator computes the similarity between \hat{P} and the intrinsic support features F_{si} . We specifically interact with the intrinsic features because they preserve the original discriminative information of the support samples.

Specifically, for the given intrinsic support features F_{si} and the fused big-capacity prototype \hat{P} , we compute a calibrated probability distribution \mathcal{P}_{cal} for each support point x over all classes $l \in \mathcal{C}$:

$$\mathcal{P}_{cal}(x, l) = \frac{\exp \left(\frac{F_{si, x} \cdot \hat{P}^l}{\|F_{si, x}\| \cdot \|\hat{P}^l\|} \right)}{\sum_{m \in \mathcal{C}} \exp \left(\frac{F_{si, x} \cdot \hat{P}^m}{\|F_{si, x}\| \cdot \|\hat{P}^m\|} \right)} \quad (17)$$

where $F_{si,x}$ is the intrinsic feature of the x -th support point, \hat{P}^l is the final prototype for class l .

The calibration loss \mathcal{L}_{cal} is then formulated as the cross-entropy loss between this predicted probability distribution and the ground-truth support mask Y_s :

$$\mathcal{L}_{\text{cal}} = -\frac{1}{N_s} \sum_{x=1}^{N_s} \sum_{l \in \mathcal{C}} Y_{s,x}^l \log(\mathcal{P}_{\text{cal}}(x, l)) \quad (18)$$

where $Y_{s,x}^i$ is the one-hot ground-truth label. The overall training objective combines this calibration loss with the main segmentation loss \mathcal{L}_{seg} , balanced by a hyperparameter λ :

$$\mathcal{L}_{\text{total}} = \mathcal{L}_{\text{seg}} + \lambda \mathcal{L}_{\text{cal}} \quad (19)$$

This mechanism effectively anchors the prototype expansion process and prevents semantic drift.

Experiment

Experiment Setup

Datasets. We evaluate our proposed PENet on two widely-used benchmark datasets for 3D few-shot semantic segmentation, S3DIS (Armeni et al. 2016) and ScanNet (Dai et al. 2017). S3DIS is composed of 272 point clouds from six large-scale indoor areas, encompassing 12 semantic categories and an additional clutter class. ScanNet is a larger and more complex collection of 1,513 scanned indoor scenes with 20 semantic categories. Following standard practice, we preprocess the raw scenes by partitioning them into 1m x 1m blocks. From each block, we then randomly sample 2048 points as input. Each point is represented by a 9-dimensional vector, including its XYZ coordinates, RGB color, and normalized spatial coordinates. For the few-shot setting, the classes in each dataset are divided into two non-overlapping splits, S0 and S1, for cross-validation. When one split is used for testing with novel classes C_{test} , the other is used for meta-training with base classes C_{train} .

Implementation Details. Our model is implemented in PyTorch and trained on NVIDIA A100 GPUs. For pre-training, IL adopts DGCNN (Wang et al. 2019) as its backbone, and the DL uses a self-supervised objective with an 80% input mask ratio, following (He et al. 2023). During meta-learning, the parameters of both the IL and DL are frozen. The remaining components are trained for 100 epochs with the Adam optimizer, an initial learning rate of 0.001, and a decay factor of 0.5 every 5K iterations. Data augmentation includes random scaling, shifting, rotation, and Gaussian jittering. The number of iterations in the PAM is set to $N=2$. The loss balancing weight λ to 1.

Comparison with State-of-the-Art Methods

Table 1 and 2 shows the experimental results of our method compared with state-of-the-art (SOTA) approaches including FT (Zhao, Chua, and Lee 2021), AttMPTI (Zhao, Chua, and Lee 2021), BFG (Mao et al. 2022), 2CBR (Zhu et al. 2023), PAP3D (He et al. 2023), SQFI (Zheng et al. 2024a), and Seg-PN (Zhu et al. 2024).

Results on S3DIS: As shown in Table 1, we compare PENet with state-of-the-art (SOTA) methods on the S3DIS dataset. Our proposed PENet consistently establishes new

SOTA performance across most few-shot settings. Specifically, in the challenging 2-way 1-shot and 3-way 1-shot scenarios, PENet achieves average mIoUs of 70.04% and 63.07%, surpassing the previous best method, Seg-PN, by significant margins of +3.63% and +1.40%, respectively. The performance gains become more pronounced in the 5-shot settings, where PENet achieves 75.31% and 68.67% mIoU in the 2-way and 3-way scenarios, surpassing Seg-PN by substantial margins of +5.95% and +5.11%. This demonstrates the superior effectiveness of our prototype expansion approach. Notably, we observe that PENet exhibits a wider performance gap between the two splits, with significantly higher scores on the S1 split compared to S0. This trend suggests that our prototype expansion mechanism effectively enhances generalization. By training on the more morphologically complex classes in the S0 split (e.g., bookcase, chair), the resulting big-capacity prototype develops a superior capability to reconcile high intra-class diversity. This enhanced capability subsequently leads to stronger segmentation performance when evaluated on the novel classes in the S1 split.

Results on ScanNet: Table 2 shows that PENet’s superior performance is further validated on the more challenging ScanNet dataset. In the 2-way 1-shot setting, our method achieves an average mIoU of 68.86%, significantly outperforming the previous state-of-the-art, Seg-PN, by +5.12%. The performance gains are consistent across all scenarios, including a notable +4.26% improvement in the 2-way 5-shot setting. These substantial improvements on a complex dataset with a wider variety of classes underscore the robust generalization capability of our approach, which effectively leverages complementary features to better understand novel scenes.

Ablation Experiments

Impact of Different Modules. We conduct a component-wise ablation study to validate the effectiveness of each key module in PENet. Table 3 presents the results under the 2-way 1-shot setting, where uppercase suffixes from A to F denote different variants of our model.

We observe that the absence of either the Diffusion Learner (DL) or the Prototype Assimilation Module (PAM) leads to a significant decline in performance. Specifically, removing the DL (PENet-A) or the PAM (PENet-B) from the full model results in a sharp mIoU drop of 7.03% and 5.84%, respectively. This aligns with our analysis in Section I, confirming that the DL is critical for providing generalizable features to address intra-class diversity, and the PAM is essential for resolving inter-set inconsistency by aligning prototypes. The optimal performance of 70.04% mIoU is achieved when all modules are integrated (PENet-F), validating the powerful synergistic effect of our complete architecture.

Ablation Study of PAM Structure. We further analyze the internal structure of our PAM to validate the contributions of its core components. The study includes ablating its symmetric push-pull blocks and varying the number of assimilation iterations, with results presented in Table 4 and Table 5, respectively.

1) Impact of Push-Pull Blocks. Table 4 shows the results of using only the push block, only the pull block, or the com-

| Methods | Venue | 2-way 1-shot | | | 2-way 5-shot | | | 3-way 1-shot | | | 3-way 5-shot | | |
|--------------|----------|--------------|--------------|---------------------|--------------|--------------|---------------------|--------------|--------------|---------------------|--------------|--------------|---------------------|
| | | S0 | S1 | Avg | S0 | S1 | Avg | S0 | S1 | Avg | S0 | S1 | Avg |
| FT | CVPR 21 | 36.34 | 38.79 | 37.57 | 56.49 | 56.99 | 56.74 | 30.05 | 32.19 | 31.12 | 46.88 | 47.57 | 47.23 |
| AttMPTI | CVPR 21 | 53.77 | 55.94 | 54.86 | 61.67 | 67.02 | 64.35 | 45.18 | 49.27 | 47.23 | 54.92 | 56.79 | 55.86 |
| BFG | 3DV 22 | 42.15 | 40.52 | 41.34 | 51.23 | 49.39 | 50.31 | 34.12 | 31.98 | 33.05 | 46.25 | 41.38 | 43.82 |
| 2CBR | TMM 23 | 55.89 | 61.99 | 58.94 | 63.55 | 67.51 | 65.53 | 46.51 | 53.91 | 50.21 | 55.51 | 58.07 | 56.79 |
| PAP3D | TIP 23 | 59.45 | 66.08 | 62.76 | 65.40 | 70.30 | 67.85 | 48.99 | 56.57 | 52.78 | 61.27 | 60.81 | 61.04 |
| SQFI | TCSVT 24 | 58.89 | 57.21 | 58.05 | 65.98 | 67.54 | 66.76 | 52.89 | 55.04 | 53.96 | 58.96 | 62.83 | 60.89 |
| Seg-PN | CVPR 24 | 64.84 | 67.98 | 66.41 | 67.63 | 71.48 | 69.36 | 60.12 | 63.22 | 61.67 | 62.58 | 64.53 | 63.56 |
| PENet (ours) | – | 65.13 | 74.94 | 70.04(+3.63) | 71.24 | 79.37 | 75.31(+5.95) | 57.03 | 69.10 | 63.07(+1.40) | 64.02 | 73.31 | 68.67(+5.11) |

Table 1: Results on S3DIS Dataset using Mean-IoU Metric (%). S_i denotes that split i is used for testing. The best results are shown in **bold**.

| Methods | Venue | 2-way 1-shot | | | 2-way 5-shot | | | 3-way 1-shot | | | 3-way 5-shot | | |
|--------------|----------|--------------|--------------|---------------------|--------------|--------------|---------------------|--------------|--------------|---------------------|--------------|--------------|---------------------|
| | | S0 | S1 | Avg | S0 | S1 | Avg | S0 | S1 | Avg | S0 | S1 | Avg |
| FT | CVPR 21 | 31.55 | 28.94 | 30.25 | 42.71 | 37.24 | 39.98 | 23.99 | 19.10 | 21.55 | 34.93 | 28.10 | 31.52 |
| AttMPTI | CVPR 21 | 42.55 | 40.83 | 41.69 | 54.00 | 50.32 | 52.16 | 35.23 | 30.72 | 32.98 | 46.74 | 40.80 | 43.77 |
| BFG | 3DV 22 | 42.15 | 40.52 | 41.34 | 51.23 | 49.39 | 50.31 | 34.12 | 31.98 | 33.05 | 46.25 | 41.38 | 43.82 |
| 2CBR | TMM 23 | 50.73 | 47.66 | 49.20 | 52.35 | 47.14 | 49.75 | 47.00 | 46.36 | 46.68 | 45.06 | 39.47 | 42.27 |
| PAP3D | TIP 23 | 57.08 | 66.08 | 55.94 | 56.51 | 64.55 | 62.10 | 55.27 | 55.60 | 55.44 | 59.02 | 53.16 | 56.09 |
| SQFI | TCSVT 24 | 56.76 | 53.32 | 55.04 | 64.79 | 59.27 | 62.03 | 55.86 | 50.17 | 53.17 | 59.30 | 56.34 | 57.82 |
| Seg-PN | CVPR 24 | 63.15 | 64.32 | 63.74 | 67.08 | 69.05 | 68.07 | 61.80 | 65.34 | 63.57 | 62.94 | 68.26 | 65.60 |
| PENet (ours) | – | 68.41 | 69.31 | 68.86(+5.12) | 73.15 | 71.51 | 72.33(+4.26) | 65.76 | 68.03 | 66.90(+3.33) | 70.55 | 69.51 | 70.03(+4.43) |

Table 2: Results on ScanNet Dataset using Mean-IoU Metric (%). S_i denotes that split i is used for testing. The best results are shown in **bold**.

| Method | IL | DL | PAM | PCM | S0 | S1 | Avg |
|---------|----|----|-----|-----|--------------|--------------|--------------|
| PENet-A | ✓ | | ✓ | ✓ | 60.05 | 65.96 | 63.01 |
| PENet-B | ✓ | ✓ | | ✓ | 61.27 | 67.12 | 64.20 |
| PENet-C | ✓ | ✓ | ✓ | | 63.40 | 72.17 | 67.79 |
| PENet-D | ✓ | | | ✓ | 55.26 | 58.33 | 56.80 |
| PENet-E | ✓ | | ✓ | | 59.94 | 63.55 | 61.75 |
| PENet-F | ✓ | ✓ | ✓ | ✓ | 65.13 | 74.94 | 70.04 |

Table 3: Effect of different modules on S3DIS under 2-way-1-shot settings.

| PAM variants | S0 | S1 | Avg |
|------------------------|--------------|--------------|--------------|
| Push block only | 63.94 | 66.42 | 65.18 |
| Pull block only | 60.72 | 72.20 | 66.46 |
| Push-pull block (ours) | 65.13 | 74.94 | 70.04 |

Table 4: Effect of push-pull block structure of PAM on S3DIS.

plete push-pull mechanism. The results indicate that both blocks are indispensable, as removing either one leads to a noticeable performance drop. Specifically, the pull block, which refines the intrinsic prototypes, appears more critical for performance on the S0 split, while the push block, which calibrates the diffusion prototypes, is more crucial for the S1 split. The full push-pull mechanism achieves the best result of 70.04% mIoU, demonstrating that the joint two complementary forces is necessary to effectively assimilate both prototype sets into the query distribution.

2) Impact of Iteration Number. We also investigate the impact of the iterative corrective force in PAM by varying

| M | S0 | S1 | Avg |
|-----|--------------|--------------|--------------|
| 1 | 62.02 | 72.42 | 67.22 |
| 2 | 65.13 | 74.94 | 70.04 |
| 3 | 62.84 | 73.29 | 68.07 |

Table 5: Effect of iteration number M of push-pull blocks in PAM.

the number of stacked push-pull blocks. The results in Table 5 show that a single iteration ($M = 1$) yields a 2.82% mIoU drop, suggesting the corrective force is insufficient to bridge the significant gap between the support-derived prototypes and the query space. Conversely, increasing the iterations to $M = 3$ appears to cause over-correction, which also degrades performance by 1.97%. The optimal performance is achieved with $M = 2$, demonstrating that this configuration strikes the best balance for effective prototype assimilation.

Generalizability Validation on N-Way Settings. To validate the generalization capability endowed by our big-capacity prototype, we evaluate PENet on more challenging N-way settings. While most existing methods limit their evaluation to 2-way or 3-way tasks, we extend our analysis up to 6-way segmentation to test the model’s robustness as the number of novel classes increases. Figure 4 illustrates the performance of PENet on the S3DIS S1 split for both 1-shot and 5-shot scenarios. Notably, even in the highly challenging 6-way 1-shot setting, our model maintains a robust performance of over 50% mIoU. This demonstrates that the expanded representational capacity of our method provides strong generalization.

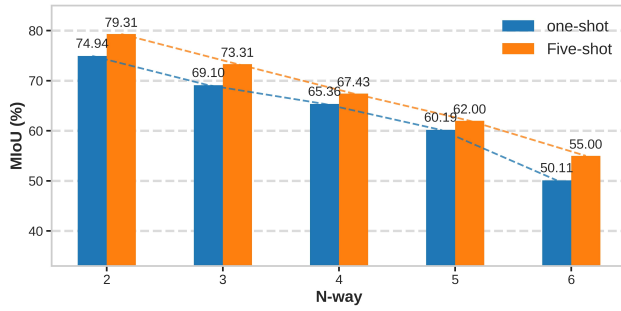


Figure 4: Model generalizability validation through N-way setting on S3DIS S1 test split performance.

Conclusion

In this paper, we propose the PENet to solve the challenges of intra-class diversity and inter-set inconsistency in few-shot 3D segmentation. PENet constructs big-capacity prototypes by using a dual-stream architecture to extract complementary representative and generalizable features from an Intrinsic Learner and a repurposed Diffusion Learner, respectively. These dual prototypes are then aligned by the PAM and regularized by the PCM. Experiments show that PENet establishes a new state-of-the-art on the S3DIS and ScanNet benchmarks. Our work validates the prototype expansion approach and highlights the value of using generative model components for discriminative few-shot learning.

References

- An, Z.; Sun, G.; Liu, Y.; Liu, F.; Wu, Z.; Wang, D.; Van Gool, L.; and Belongie, S. 2024. Rethinking few-shot 3d point cloud semantic segmentation. In *Proceedings of the IEEE/CVF Conference on Computer Vision and Pattern Recognition*, 3996–4006.
- Armeni, I.; Sener, O.; Zamir, A. R.; Jiang, H.; Brilakis, I.; Fischer, M.; and Savarese, S. 2016. 3d semantic parsing of large-scale indoor spaces. In *Proceedings of the IEEE/CVF Conference on Computer Vision and Pattern Recognition*, 1534–1543.
- Bar, A.; Maimon, Y.; and Gafni, Y. 2022. Visual prompting via image inpainting. In *Advances in Neural Information Processing Systems*, volume 35, 32800–32813.
- Dai, A.; Chang, A. X.; Savva, M.; Halber, M.; Funkhouser, T.; and Nießner, M. 2017. Scannet: Richly-annotated 3d reconstructions of indoor scenes. In *Proceedings of the IEEE/CVF Conference on Computer Vision and Pattern Recognition*, 5828–5839.
- Fei, H.; Wu, S.; Zhang, M.; Zhang, M.; Chua, T.-S.; and Yan, S. 2024. Enhancing video-language representations with structural spatio-temporal alignment. In *Proceedings of the IEEE/CVF Conference on Computer Vision and Pattern Recognition*.
- Gandikota, R.; O’Brien, J.; Zhang, J.; Bao, J.; and Bablani, B. 2023. Erasing concepts from diffusion models. *arXiv preprint arXiv:2303.07345*.
- He, S.; Jiang, X.; Jiang, W.; and Ding, H. 2023. Prototype adaption and projection for few-and zero-shot 3d point cloud semantic segmentation. *IEEE Transactions on Image Processing*, 32: 3199–3211.
- Ho, J.; Jain, A.; and Abbeel, P. 2020. Denoising diffusion probabilistic models. In *Advances in Neural Information Processing Systems*, volume 33, 6840–6851.
- Hu, X.; Zhong, B.; Liang, Q.; Zhang, S.; Li, N.; and Li, X. 2024. Towards Modalities Correlation for RGB-T Tracking. *IEEE Transactions on Circuits and Systems for Video Technology*.
- Huang, X.; Lin, J.; Chen, J.; Ma, X.; Chen, B.; and Lu, G. 2024. Progressive Stepwise Diffusion Model with Dual Decoders for Semi-Supervised Medical Image Segmentation. In *2024 IEEE International Conference on Bioinformatics and Biomedicine (BIBM)*, 2060–2067.
- Huang, Y.; Lei, Y.; Han, J.; and Xu, L. 2023. Part-aware prototypical network for few-shot 3d point cloud semantic segmentation. In *Proceedings of the AAAI Conference on Artificial Intelligence*, volume 37, 1017–1025.
- Lai, X.; Liu, J.; Jiang, L.; Wang, L.; Zhao, H.; Liu, S.; Qi, X.; and Jia, J. 2022. Stratified transformer for 3d point cloud segmentation. In *Proceedings of the IEEE/CVF Conference on Computer Vision and Pattern Recognition*, 8500–8509.
- Li, A. C.; Prabhudesai, M.; Duggal, S.; Brown, E.; and Pathak, D. 2023. Your diffusion model is secretly a zero-shot classifier. In *Proceedings of the IEEE/CVF International Conference on Computer Vision*, 2206–2217.
- Li, Y.; Yu, K.; Yang, F.; Shen, C.; Chang, J.; Li, Z.; and Liu, K. 2025. Hierarchical feature-guided prototypical network for few-shot knowledge graph completion. *Neural Networks*, 107702.
- Lyu, X.; Lin, P.; Dai, C.; and Li, C. 2022. Lion: Latent point diffusion models for 3d shape generation. In *Advances in Neural Information Processing Systems*, volume 35, 3328–3341.
- Mao, Y.; Guo, Z.; Xiaonan, L. I. U.; Yuan, Z.; and Guo, H. 2022. Bidirectional Feature Globalization for Few-shot Semantic Segmentation of 3D Point Cloud Scenes. In *International Conference on 3D Vision*, 505–514.
- Nichol, A.; Jun, H.; Dhariwal, P.; Mishkin, P.; and Chen, M. 2022. Point-e: A system for generating 3d point clouds from complex prompts. *arXiv preprint arXiv:2212.08751*.
- Nichol, A. Q.; and Dhariwal, P. 2021. Improved denoising diffusion probabilistic models. In *International Conference on Machine Learning*, 8162–8171.
- Ning, Z.; Tian, Z.; Lu, G.; and Pei, W. 2023. Boosting few-shot 3d point cloud segmentation via query-guided enhancement. In *Proceedings of the ACM International Conference on Multimedia*, 1895–1904.
- Peebles, W.; and Xie, S. 2023. Scalable diffusion models with transformers. In *Proceedings of the IEEE/CVF International Conference on Computer Vision*, 4195–4205.
- Sereno, M.; Wang, X.; Besançon, L.; McGuffin, M. J.; and Isenberg, T. 2020. Collaborative work in augmented reality: A survey. *IEEE transactions on visualization and computer graphics*, 28(6): 2530–2549.
- Snell, J.; Swersky, K.; and Zemel, R. 2017. Prototypical networks for few-shot learning. In *Advances in Neural Information Processing Systems*, 4077–4087.

Soori, M.; Arezoo, B.; and Dastres, R. 2023. Artificial intelligence, machine learning and deep learning in advanced robotics, a review. *Cognitive Robotics*, 3: 54–70.

Vinyals, O.; Blundell, C.; Lillicrap, T.; Kavukcuoglu, K.; and Wierstra, D. 2016. Matching networks for one shot learning. In *Advances in Neural Information Processing Systems*, 3630–3638.

Wang, R.; Lam, S.-K.; Wu, M.; Hu, Z.; Wang, C.; and Wang, J. 2025. Destination intention estimation-based convolutional encoder-decoder for pedestrian trajectory multimodality forecast. *Measurement*, 239: 115470.

Wang, Y.; Sun, Y.; Liu, Z.; Sarma, S. E.; Bronstein, M. M.; and Solomon, J. M. 2019. Dynamic graph cnn for learning on point clouds. *ACM Transactions on Graphics (tog)*, 38(5): 1–12.

Yu, Z.; Chang, H.; Yu, Z.; Guo, B.; and Shi, R. 2021. Location selection for air quality monitoring with consideration of limited budget and estimation error. *IEEE Transactions on Mobile Computing*, 21(11): 4025–4037.

Zhang, C.; Wu, Z.; Wu, X.; Zhao, Z.; and Wang, S. 2023. Few-shot 3d point cloud semantic segmentation via stratified class-specific attention based transformer network. In *Proceedings of the AAAI Conference on Artificial Intelligence*, volume 37, 3410–3417.

Zhang, H.; Wang, C.; Yu, L.; Tian, S.; Ning, X.; and Rodrigues, J. 2024. PointGT: A Method for Point-Cloud Classification and Segmentation Based on Local Geometric Transformation. *IEEE Transactions on Multimedia*.

Zhang, L.; Rao, A.; and Agrawala, M. 2023. Adding conditional control to text-to-image diffusion models. In *Proceedings of the IEEE/CVF International Conference on Computer Vision*, 3836–3847.

Zhao, N.; Chua, T.-S.; and Lee, G. H. 2021. Few-shot 3d point cloud semantic segmentation. In *Proceedings of the IEEE/CVF Conference on Computer Vision and Pattern Recognition*, 8873–8882.

Zhao, Y.; Li, A.; Du, Z.; Chen, Y.; Sun, H.; and Zhi, Z. 2024. Joint structure detection and multi-scale clustering filtering for tunnel lining extraction from point clouds. *IEEE Transactions on Intelligent Transportation Systems*, 25(9): 11214–11226.

Zheng, C.; Liu, L.; Meng, Y.; Peng, X.; and Wang, M. 2024a. Few-shot point cloud semantic segmentation via support-query feature interaction. *IEEE Transactions on Circuits and Systems for Video Technology*, 34(11): 10753–10763.

Zheng, X.; Huang, X.; Mei, G.; Hou, Y.; Lyu, Z.; Dai, B.; Ouyang, W.; and Gong, Y. 2024b. Point cloud pre-training with diffusion models. In *Proceedings of the IEEE/CVF Conference on Computer Vision and Pattern Recognition*, 22935–22945.

Zhu, G.-Z.; Zhou, Y.-T.; Yao, R.; and Zhu, H. 2023. Cross-class bias rectification for point cloud few-shot segmentation. *IEEE Transactions on Multimedia*.

Zhu, X.; Zhang, R.; He, B.; Guo, Z.; Liu, J.; Xiao, H.; Fu, C.; Dong, H.; and Gao, P. 2024. No Time to Train: Empowering Non-Parametric Networks for Few-shot 3D Scene Segmentation. In *Proceedings of the IEEE/CVF Conference on Computer Vision and Pattern Recognition*, 3838–3847.